New Members of the Homologous Series $A_m[M_6Se_8]_m[M_{5+n}Se_{9+n}]$: The Quaternary Phases $A_{1-x}M'_{3-x}Bi_{11+x}Se_{20}$ and $A_{1+x}M'_{3-2x}Bi_{7+x}Se_{14}$ (A = K, Rb, Cs; M′ = Sn, Pb)

Antje Mrotzek, Lykourgos Iordanidis, and Mercouri G. Kanatzidis*

Department of Chemistry and Center for Fundamental Materials Research, Michigan State University, East Lansing, Michigan 48824

Received March 15, 2001

The compounds $A_{1+x}M'_{3-2x}Bi_{7+x}Se_{14}$ and $A_{1-x}M'_{3-x}Bi_{11+x}Se_{20}$ (A = K, Rb, Cs; M′ = Sn, Pb) were discovered from reactions involving A_2Se, Bi_2Se_3, M′, and Se at 760 °C. The single-crystal structures reveal that $A_{1+x}M'_{3-2x}Bi_{7+x}Se_{14}$ are isostructural to $K_{2.5}Bi_{8.5}Se_{14}$ whereas $A_{1-x}M'_{3-x}Bi_{11+x}Se_{20}$ adopt a new structure type. Both compound types belong to the homologous series $A_m[M_6Se_8]_m[M_{5+n}Se_{9+n}]$ (M = di- and trivalent metal), whose characteristics are three-dimensional anionic frameworks with tunnels filled with alkali ions. The building units are derived from different sections of the NaCl lattice, perpendicular to the [111] ($NaCl^{111}$-type) and [100] ($NaCl^{100}$-type) directions, respectively, with dimensions and shapes defined by *m* and *n*. The structures of $A_{1+x}M'_{3-2x}Bi_{7+x}Se_{14}$ ($m = 2$, $n = 3$) and $A_{1-x}M'_{3-x}Bi_{11+x}Se_{20}$ ($m = 1$, $n = 3$) exhibit the same type of step-shaped $NaCl^{111}$-type layer but differ in the size of the $NaCl^{100}$-type unit. In both structures, the Bi and Sn (Pb) atoms are extensively disordered over the metal sites of the chalcogenide network. The physicochemical and charge transport properties of $A_{1+x}M'_{3-2x}Bi_{7+x}Se_{14}$ and $A_{1-x}M'_{3-x}Bi_{11+x}Se_{20}$ (A = K, Rb, Cs; M′ = Sn, Pb) are reported.

Introduction

There is currently strong interest in developing new physicochemical concepts in designing materials with superior thermoelectric properties.[1−3] Our approach, which has been outlined in detail elsewhere,[4] is focused on complex quaternary and ternary bismuth chalcogenides with "derivatized" Bi_2Te_3-type frameworks. The derivatization is brought about through the incorporation of alkali metals. The strategy aims to exploit the beneficial effects of structural complexity and mass fluctuation phonon scattering on the thermopower and thermal conductivity, respectively.[4] The examples of $CsBi_4Te_6$[5,6] and β-$K_2Bi_8Se_{13}$[6,7] show that these exploratory investigations can lead to promising thermoelectric materials with promising properties. Therefore, we expanded our investigations to quaternary systems to further explore the effects of structural complexity and mass fluctuation on the physical properties. The investigation of the systems A/Pb/Bi/Se (A = K, Rb, Cs, Sr, Ba, Eu) led to the compounds $K_{1.25}Pb_{3.5}Bi_{7.25}Se_{15}$,[8] $RbPbBi_3Se_6$, α- and β-$CsPbBi_3Se_6$,[9] $Sr_2Pb_2Bi_6Se_{13}$,[6] $Ba_3Pb_3Bi_6Se_{15}$,[10] $Ba_3PbBi_6Se_{13}$,[11] and $Eu_2Pb_2Bi_6Se_{13}$.[6] These phases exhibit an impressive structural diversity that is characterized by modular construction achieved by combining fragments excised out of the Bi_2Te_3 and NaCl lattices. $K_{1.25}Pb_{3.5}Bi_{7.25}Se_{15}$ shows promising thermoelectric properties and belongs to a broad class of quaternary solids with the general formula $A_{1+x}M'_{4-2x}M''_{7+x}Se_{15}$ (A = K, Rb; M′ = Pb, Sn; M″ = Bi, Sb).[8]

Recently we also described $K_{1-x}Sn_{4-x}Bi_{11+x}Se_{21}$,[12] $K_{1-x}Sn_{5-x}Bi_{11+x}Se_{22}$,[13] and $K_{1+x}Sn_{4-2x}Bi_{7+x}Se_{15}$,[8] which have structures

(1) (a) Slack, G. A. In *CRC Handbook of Thermoelectrics*; Rowe, D. M., Ed.; CRC Press: Boca Raton, 1995; pp 407−440. (b) Slack, G. A. In *Solid State Physics*; Ehrenreich, H., Seitz, F., Turnbull, D., Eds.; Academic: New York, 1997; Vol. 34, p 1. (c) Sales, B. C. *Mater. Res. Bull.* **1998**, *23*, 15−21. (d) Sales, B. C.; Mandrus, D.; Chakoumakos, B. C.; Keppens, V.; Thompson, J. R.; *Phys. Rev. B* **1997**, *56*, 15081−15089. (e) Tritt, T. M. *Science* **1996**, *272*, 1276−1277.

(2) (a) Tritt, T. M., Kanatzidis, M. G., Mahan, G. D., Lyon, H. B., Eds. Thermoelectric Materials 1998—The Next Generation Materials for Small-Scale Refrigeration and Power Applications. *Mater. Res. Soc. Symp. Proc.* **1998**, Vol. 545, see papers in this volume. (b) Tritt, T. M., Kanatzidis, M. G., Lyon, H. B., Mahan, G. D., Eds. Thermoelectric Materials—New Directions and Approaches. *Mater. Res. Soc. Symp. Proc.* **1997**, Vol. 478, see papers in this volume.

(3) *CRC Handbook of Thermoelectrics*; Rowe, D. M., Ed.; CRC Press: Boca Raton, 1995. (b) Hicks, L. D.; Dresselhaus, M. S. *Phys. Rev. B* **1993**, *47*, 12727−12731. (c) Hicks, L. D.; Dresselhaus, M. S. *Phys. Rev. B* **1993**, *47*, 16631−16634. (d) Hicks, L. D.; Harmann, T. C.; Dresselhaus, M. S. *Appl. Phys. Lett.* **1993**, *63*, 3230−3232. (e) Broido, D. A.; Reinecke, T. L. *Appl. Phys. Lett.* **1995**, *67*, 1170−1171. (f) Sofo, J. O.; Mahan, G. D. *Appl. Phys. Lett.* **1994**, *65*, 2690−2692.

(4) (a) Kanatzidis, M. G.; DiSalvo, F. J. *ONR Q. Rev.* **1996**, *27*, 14−22. (b) Chung, D.-Y.; Iordanidis, L.; Choi, K.-S.; Kanatzidis, M. G. *Bull. Korean Chem. Soc.* **1998**, *19*, 1283−1293. (c) Kanatzidis, M. G. *Semicond. Semimet.* **2001**, *69*, 51−100.

(5) Chung, D.-Y.; Hogan, T.; Brazis, P. W.; Rocci-Lane, M.; Kannewurf, C. R.; Bastea, M.; Uher, C.; Kanatzidis, M. G. *Science* **2000**, *287*, 1024−1027.

(6) (a) Kanatzidis, M. G.; Chung, D.-Y.; Iordanidis, L.; Choi, K.-S.; Brazis, P.; Rocci, M.; Hogan, T.; Kannewurf, C. *Mater. Res. Soc. Symp. Proc.* **1998**, *545*, 233−246. (b) Bravis, P. W.; Rocci-Lane, M. A.; Ireland, J. R.; Chung, D.-Y.; Kanatzidis, M. G.; Kannewurf, C. R. *Proc. XVIIIth Int. Conf. Thermoelectrics (ITC '99)*, Baltimore, **1999**, 619−622.

(7) (a) Kanatzidis, M. G.; McCarthy, T. J.; Tanzer, T. A.; Chen, L.-H.; Iordanidis, L.; Hogan, T.; Kannewurf, C. R.; Uher, C.; Chen, B. *Chem. Mater.* **1996**, *8*, 1465−1474. (b) Chen, B.; Uher, C.; Iordanidis, L.; Kanatzidis, M. G. *Chem. Mater.* **1997**, *9*, 1655−1658.

(8) Choi, K.-S.; Chung, D.-Y.; Mrotzek, A.; Brazis, P.; Kannewurf, C. R.; Uher, C.; Chen, W.; Hogan, T.; Kanatzidis, M. G. *Chem. Mater.* **2001**, *13*, 756−764.

(9) Chung, D.-Y.; Iordanidis, L.; Rangan, K. K.; Brazis, P. W.; Kannewurf, C. R.; Kanatzidis, M. G. *Chem. Mater.* **1999**, *11*, 1352−1362.

(10) Iordanidis, L.; Kanatzidis, M. G. To be published.

(11) (a) Wang, Y.-C.; DiSalvo, F. J. *Chem. Mater.* **2000**, *12*, 1011−1017. (b) Iordanidis, L.; Bravis, P. W.; Kannewurf, C. R.; Kanatzidis, M. G. *Mater. Res. Soc. Symp. Proc.* **1998**, *545*, 189−196.

(12) Mrotzek, A.; Chung, D.-Y.; Hogan, T.; Kanatzidis, M. G. *J. Mater. Chem.* **2000**, *10*, 1667−1672.

(13) Mrotzek, A.; Chung, D.-Y.; Ghelani, N.; Hogan, T.; Kanatzidis, M. G. *Chem. Eur. J.* **2001**, *7*, 1915−1926.

10.1021/ic010285w CCC: $20.00
Published on Web 10/26/2001

closely related to each other and to those of β-$K_2Bi_8Se_{13}$ and $K_{2.5}Bi_{8.5}Se_{14}$.[14] They are all members of a newly identified grand homologous series $A_m[M_6Se_8]_m[M_{5+n}Se_{9+n}]$[12] (M = di- and trivalent metal) in both a compositional and structural sense. Their structures are composed of $[M_{5+n}Se_{9+n}]$ ($NaCl^{111}$-type) and $[M_6Se_8]_m$ ($NaCl^{100}$-type) units[15] of variable dimensions defined by *n* and *m*, which link to produce anionic frameworks with alkali metal (A_m) filled tunnels. The existence of the homologous series was recognized *after* these compounds were discovered and structurally characterized. The series however has predictive properties, and here we describe several new members that in fact were targeted for synthesis based on the general formula $A_m[M_6Se_8]_m[M_{5+n}Se_{9+n}]$ with $m = 2$, $n = 3$ and $m = 1$, $n = 3$. We report on the crystal structure and charge transport properties of $K_{1+x}Sn_{3-2x}Bi_{7+x}Se_{14}$, $K_{1+x}Pb_{3-2x}Bi_{7+x}Se_{14}$, $Cs_{1+x}Sn_{3-2x}Bi_{7+x}Se_{14}$, $Cs_{1+x}Pb_{3-2x}Bi_{7+x}Se_{14}$, $K_{1-x}Sn_{3-x}Bi_{11+x}Se_{20}$, $K_{1-x}Pb_{3-x}Bi_{11+x}Se_{20}$, $Rb_{1-x}Sn_{3-x}Bi_{11+x}Se_{20}$, $Rb_{1-x}Pb_{3-x}Bi_{11+x}Se_{20}$, $Cs_{1-x}Sn_{3-x}Bi_{11+x}Se_{20}$, and $Cs_{1-x}Pb_{3-x}Bi_{11+x}Se_{20}$ and discuss their relationship to the known members of the $A_m[M_6Se_8]_m[M_{5+n}Se_{9+n}]$ series.

Experimental Section

Synthesis. All manipulations were carried out under a dry nitrogen atmosphere in a Vacuum Atmospheres Dri-Lab glovebox. The starting material Bi_2Se_3 was obtained by reaction of stoichiometric amounts of the elements (99.999% purity) in evacuated quartz glass ampules at 800 °C for 3 days. The alkali selenide A_2Se (A = K, Rb, Cs) was prepared by stoichiometric reaction of alkali metal and selenium in liquid ammonia.

$A_{1+x}M'_{3-2x}Bi_{7+x}Se_{14}$ (A = K, Cs; M′ = Sn, Pb). A mixture of A_2Se (1 mmol), M′ (7 mmol), Se (7 mmol), and Bi_2Se_3 (7 mmol) was loaded in a carbon-coated quartz tube (9 mm diameter) and sealed at a residual pressure of $<10^{-4}$ Torr. The starting materials were heated within 24 h to 800 °C and kept there for 24 h, followed by slow cooling to 50 °C at a rate of 0.5 °C/min. A silver, shiny, polycrystalline ingot of pure $A_{1+x}M'_{3-2x}Bi_{7+x}Se_{14}$ was obtained after washing any impurities with dimethylformamide (DMF), methanol, and diethyl ether. A quantitative microprobe analysis with a SEM/EDS system performed on different crystals gave the following average compositions: $K_{1.8}Sn_{2.1}Bi_{7.8}Se_{14}$, $K_{1.6}Pb_{2.3}Bi_{8.0}Se_{14}$, $Cs_{1.1}Sn_{1.9}Bi_{7.9}Se_{14}$, and $Cs_{1.0}Sn_{2.7}Bi_{7.6}Se_{14}$, respectively.

$A_{1-x}M'_{3-x}Bi_{11+x}Se_{20}$ (A = K, Rb, Cs; M′ = Sn, Pb). A mixture of A_2Se (1 mmol), M′ (3 mmol), Se (3 mmol), and Bi_2Se_3 (5.5 mmol) was loaded in a carbon-coated quartz tube (9 mm diameter) and sealed at a residual pressure of $<10^{-4}$ Torr. The starting materials were heated within 12 h to 800 °C and kept there for 24 h, followed by slow cooling to 400 °C at a rate of 0.1 °C/min and then to 50 °C in 10 h. A silver, shiny, polycrystalline ingot of $A_{1-x}M'_{3-x}Bi_{11+x}Se_{20}$ was obtained after washing any impurities with dimethylformamide (DMF), methanol, and diethyl ether. A quantitative microprobe analysis with a SEM/EDS system performed on different crystals gave the following average compositions: $K_{0.9}Sn_{2.7}Bi_{10.9}Se_{20}$, $K_{0.7}Pb_{2.8}Bi_{11.1}Se_{20}$, $Rb_{1.0}Pb_{3.5}Bi_{11.4}Se_{20}$, $Cs_{0.8}Sn_{3.1}Bi_{11.3}Se_{20}$, and $Cs_{0.7}Pb_{3.5}Bi_{10.6}Se_{20}$, respectively.

$Rb_{1-x}Sn_{3-x}Bi_{11+x}Se_{20}$. Initially the compound was synthesized the following way: A mixture of 0.040 g (0.160 mmol) of Rb_2Se, 0.734 g (1.118 mmol) of Bi_2Se_3, 0.038 g (0.320 mmol) of Sn, and 0.025 g (0.317 mmol) of Se was transferred into a carbon coated silica tube, which was flame-sealed under vacuum. The tube was heated to 760 °C in 24 h, kept at 760 °C for 3 days, cooled to 450 °C in 60 h, and further cooled to 50 °C in 11 h. The product consisted of a silvery chunk with needles growing across its surface. $Rb_{1-x}Sn_{3-x}Bi_{11+x}Se_{20}$ is the major phase with a second minor unidentified phase. Pure material can be made as follows: A mixture of 0.014 g (0.056 mmol) of Rb_2Se, 0.500 g (0.763 mmol) of Bi_2Se_3, 0.026 g (0.219 mmol) of Sn, and 0.017 g (0.215 mmol) of Se was transferred into a carbon-coated silica tube. The tube was placed under the flame of a natural gas−oxygen torch until the mixture melted, and then the tube was removed from the flame and allowed to solidify. A quantitative microprobe analysis with a SEM/EDS system performed on different crystals gave the following average composition: $Rb_{0.7}Sn_{3.2}Bi_{11.5}Se_{20}$.

Physical Measurements. Electron Microscopy. Quantitative microprobe analyses of the compounds were performed with a JEOL JSM-35C SEM equipped with a Tracor Northern EDS detector. Data were acquired using an accelerating voltage of 25 kV and a 60 s accumulation time. The quantitative microprobe analyses have a standard deviation of about 2−5%.

Differential Thermal Analysis. Differential thermal analysis (DTA) was performed with a computer-controlled Shimadzu DTA-50 thermal analyzer as described earlier.[12] The samples were heated to 900 °C at 10 °C/min and kept at this temperature (isothermed) for 5 min followed by cooling at −10 °C/min to 50 °C.

Infrared Spectroscopy. Diffuse reflectance spectra were recorded in the region 6000−400 cm^{-1} with the use of a Nicolet MAGNA-IR 750 spectrometer equipped with a collector diffuse reflectance accessory from Spectra-Tech, Inc. Band gaps were obtained as described elsewhere.[7]

Charge Transport Measurements. Room temperature conductivity measurements were performed in the usual four-probe geometry. The Seebeck coefficient was measured between 300 and 400 K by using a SB-100 Seebeck effect measurement system, MMR Technologies, Inc.

Powder X-ray Diffraction. Powder patterns of all starting materials and products were obtained using a CPS 120 INEL X-ray powder diffractometer equipped with a position-sensitive detector and graphite-monochromated Cu Kα radiation. The purity and homogeneity were confirmed by comparing the X-ray powder diffraction pattern to that calculated from single-crystal data using the CERIUS[2] software.[16]

Single-Crystal X-ray Crystallography. Single crystals of $K_{1.40}Sn_{2.20}Bi_{7.40}Se_{14}$, $K_{0.70}Sn_{2.70}Bi_{11.30}Se_{20}$, $Rb_{0.36}Sn_{2.36}Bi_{11.64}Se_{20}$, and $Cs_{0.46}Sn_{2.46}Bi_{11.54}Se_{20}$ were mounted on the tip of a glass fiber. The intensity data were collected on a Bruker SMART Platform CCD diffractometer with graphite-monochromatized Mo Kα radiation and the SMART software[17] for data acquisition. The extraction and reduction of the data were performed with the program SAINT.[18] The observed systematic absences led in each case to the space group $P2_1/m$. For the data sets of $K_{1.40}Sn_{2.20}Bi_{7.40}Se_{14}$, $K_{0.70}Sn_{2.70}Bi_{11.30}Se_{20}$, and $Cs_{0.46}Sn_{2.46}Bi_{11.54}Se_{20}$ an analytical absorption correction was performed using the program XPREP[19] followed by a semiempirical absorption correction based on symmetrically equivalent reflections with the program SADABS.[20] Only a semiempirical absorption correction was done for $Rb_{0.36}Sn_{2.36}Bi_{11.64}Se_{20}$. The crystal structures were solved with direct methods (SHELXS-97[19]) and refined using the SHELXTL package of crystallographic programs.[19]

$K_{1.40}Sn_{2.20}Bi_{7.40}Se_{14}$. Twenty-seven crystallographically independent positions (Bi1−8, Sn1−2, Se1−14 and K1−3) were found situated on mirror planes ($y = 1/4$ and $3/4$). The structure refinement revealed unusually high thermal displacement parameters for the Bi2, Bi5−7 sites which introduced a disorder model with mixed Bi/Sn occupancies in the same crystallographic site. The refinement resulted in 14% Sn in the Bi2 site, 13% Sn in the Bi5 site, 16% Sn in the Bi6 site, and 17% in the Bi7 site. High thermal displacement parameters of the Sn1−2 sites indicated less electron density than calculated. This led to

(14) Chung, D.-Y.; Choi, K.-S.; Iordanidis, L.; Schindler, J. L.; Brazis, P. W.; Kannewurf, C. R.; Chen, B.; Hu, S.; Uher, C.; Kanatzidis, M. G. *Chem. Mater.* **1997**, *9*, 3060−3071.

(15) (a) $NaCl^{111}$ is meant to indicate that this fragment derives from cutting the NaCl lattice perpendicular to the [111] direction. $NaCl^{100}$ refers to a section of the NaCl lattice derived from a cut perpendicular to the [100] direction. (b) In a previous publication,[13] we addressed the ($NaCl^{111}$) and ($NaCl^{100}$) fragments as Bi_2Te_3-type and NaCl-type, respectively. We now realize this may be inadequate for large values of *n*.

(16) *CERIUS*[2], version 1.6; Molecular Simulations, Inc.: Cambridge, England, 1994.

(17) *SMART*; Siemens Analytical X-ray Systems Inc.: Madison, WI, 1996.

(18) *SAINT V-4*; Siemens Analytical X-ray Systems Inc.: Madison, WI, 1994−1996.

(19) Sheldrick, G. M. *SHELXTL V-5*; Siemens Analytical X-ray Systems Inc.: Madison, WI, 1994.

(20) *SADABS V-4*; Siemens Analytical X-ray Systems Inc.: Madison, WI, 1994−1996.

Table 1. Summary of Crystallographic Data and Structural Analysis

chemical formula	$K_{1.40}Sn_{2.20}Bi_{7.40}Se_{14}$	$K_{0.70}Sn_{2.70}Bi_{11.30}Se_{20}$	$Rb_{0.36}Sn_{2.36}Bi_{11.64}Se_{20}$	$Cs_{0.46}Sn_{2.46}Bi_{11.54}Se_{20}$
fw	2967.75	4288.51	4322.60	4343.95
space group (No.)	$P2_1/m$	$P2_1/m$	$P2_1/m$	$P2_1/m$
a, Å	17.402(2)	16.139(2)	16.038(2)	16.100(3)
b, Å	4.2054(6)	4.1470(5)	4.1540(6)	4.1360(8)
c, Å	21.227(3)	17.009(2)	17.028(3)	17.077(3)
β, deg	109.524(2)	116.881(2)	116.517(2)	116.79(3)
Z; V, Å^3	2; 1464.1(4)	1, 1015.4(2)	1, 1015.1(3)	1, 1015.1(3)
D_{calcd}, g cm^{-3}	6.732	7,013	7.071	7.106
temp, °C	25	25	27	25
λ(Mo Kα), Å	0.71073	0.71073	0.71073	0.71073
μ(Mo Kα), cm^{-1}	63.734	68.385	70.021	69.633
R1/wR2,[a] %	3.56/6.40	3.20/5.39	5.40/14.68	5.26/11.19

[a] $R1 = \sum||F_o| - |F_c||/\sum|F_o|$, $wR2 = \{\sum[w(F_o^2 - F_c^2)^2]/\sum[w(F_o^2)^2]\}^{1/2}$.

Table 2. Fractional Atomic Coordinates ($y = 0.25$) and Equivalent Atomic Displacement Parameter (U_{eq}) Values in 10^{-3} Å^2 for $K_{1.40}Sn_{2.20}Bi_{7.40}Se_{14}$ with Estimated Standard Deviations in Parentheses

	x	z	occupancy	U_{eq}[a]
Bi1	0.09141(3)	0.98618(3)	1	19.8(1)
Bi2/Sn2′	0.71973(3)	0.06218(3)	0.862(1)/0.138	18.4(1)
Bi3	0.47670(3)	0.90710(3)	1	18.0(1)
Bi4	0.33756(3)	0.13971(3)	1	20.1(1)
Bi5/Sn5′	0.08145(3)	0.72984(3)	0.870(1)/0.130	16.6(1)
Bi6/Sn6′	0.12573(3)	0.38501(3)	0.841(1)/0.159	15.1(1)
Bi7/Sn7′	0.88949(3)	0.42845(3)	0.829(1)/0.171	15.3(1)
Bi8	0.66445(2)	0.48219(3)	1	18.8(1)
Sn1	0.82947(8)	0.78941(8)	0.771(1)	37.5(4)
K1	0.8678(9)	0.8089(9)	0.229	37.5
Sn2	0.34162(8)	0.69010(7)	0.830(1)	31.3(4)
K2	0.336(1)	0.721(1)	0.170	31.3
K3	0.5778(2)	0.6441(2)	1	37.2(9)
Se1	0.01824(7)	0.08557(6)	1	18.6(3)
Se2	0.78769(8)	0.93938(8)	1	26.1(4)
Se3	0.40080(7)	0.01565(6)	1	15.3(3)
Se4	0.17055(8)	0.87413(7)	1	19.9(3)
Se5	0.63385(7)	0.15803(6)	1	18.8(3)
Se6	0.54799(7)	0.80265(6)	1	19.0(3)
Se7	0.28434(8)	0.24668(7)	1	23.0(3)
Se8	0.02976(7)	0.25356(7)	1	19.9(3)
Se9	0.81127(7)	0.29345(7)	1	19.5(3)
Se10	0.57368(9)	0.34801(7)	1	29.3(4)
Se11	0.77947(7)	0.63749(7)	1	20.4(3)
Se12	0.99300(7)	0.58576(6)	1	15.4(3)
Se13	0.21553(7)	0.55302(7)	1	21.8(3)
Se14	0.42291(7)	0.49053(7)	1	20.5(3)

[a] U_{eq} is defined as one-third of the trace of the orthogonalized $\mathbf{U}_{ij}$ tensor.

a disorder model with mixed Sn/K occupancies in the Sn1−2 sites. The presence of high remaining electron density near these sites introduced a split model for the Sn1−2 sites with the sum of the occupancies constrained to be 1 (fully occupied) for a split position. The refinement resulted in the following occupancies: 77% and 23% for the Sn1 and K1 site, respectively, 83% and 17% for the Sn2 and K2 site, respectively. This leads to the general charge balanced formula $K_{1+x}Sn_{3-2x}Bi_{7+x}Se_{14}$ assuming the formal charges of K^+, Sn^{2+}, Bi^{3+}, and Se^{2-}. After anisotropic refinement the R1 and wR2 values dropped to 3.6% and 6.4%, respectively. The results of the structure refinements and other crystallographic data are given in Tables 1, 2, and 6.

$K_{0.70}Sn_{2.70}Bi_{11.30}Se_{20}$. Eighteen crystallographically independent positions (Bi1−6, Sn1, Se1−10 and K1) were found situated on mirror planes ($y = 1/4$ and $3/4$). The structure refinement revealed relatively high thermal displacement parameters for the Bi2−6 sites, which introduced a disorder model with mixed Bi/Sn occupancies for these sites. The refinement resulted in small but significant amounts (between 2% and 4%) of Sn in the Bi2−4 sites. Sn is accumulated in the Bi5 and Bi6 sites with 23% Sn and 11% Sn, respectively. An unusual thermal displacement parameter of the Sn1 site indicated higher electron density in this site which led to a mixed-occupancy model between Sn and Bi. The refinement converged at 10% Bi in the Sn1 site. The thermal displacement parameter of the K1 site remained high with 135 Å^2 even after the refinement of the occupancy of this site that converged to 0.35(1), i.e., equal to about $1/3$ occupied. This leads to the general

Table 3. Fractional Atomic Coordinates ($y = 0.25$) and Equivalent Atomic Displacement Parameter (U_{eq}) Values in 10^{-3} Å^2 for $K_{0.70}Sn_{2.70}Bi_{11.30}Se_{20}$ with Estimated Standard Deviations in Parentheses

	x	z	occupancy	U_{eq}[a]
Bi1	0.61134(5)	0.08257(4)	1	22.0(1)
Bi2/Sn2′	0.14917(5)	0.73635(4)	0.960(5)/0.040	21.2(2)
Bi3/Sn3′	0.08980(5)	0.45083(4)	0.962(5)/0.038	18.7(2)
Bi4/Sn4′	0.67808(5)	0.36766(4)	0.973(5)/0.027	22.5(2)
Bi5/Sn5′	0.18244(6)	0.24181(4)	0.766(5)/0.234	27.1(2)
Bi6/Sn6′	0.89378(5)	0.00127(4)	0.885(5)/0.115	21.7(2)
Sn1/Bi1′	0.59625(9)	0.78650(8)	0.896(5)/0.104	38.4(5)
K1	0.490(1)	0.502(1)	0.35(1)	135(11)
Se1	0.4186(1)	0.04448(9)	1	20.4(3)
Se2	0.8178(1)	0.1391(1)	1	21.0(4)
Se3	0.9429(1)	0.67410(9)	1	19.8(3)
Se4	0.2850(1)	0.50409(9)	1	20.3(3)
Se5	0.4950(1)	0.3323(1)	1	36.9(4)
Se6	0.3514(1)	0.77551(9)	1	21.5(4)
Se7	0.8856(1)	0.40700(9)	1	17.2(3)
Se8	0.6905(1)	0.6822(1)	1	22.6(4)
Se9	0.9741(1)	0.88813(9)	1	18.1(3)
Se10	0.2343(1)	0.10949(9)	1	20.0(3)

[a] U_{eq} is defined as one-third of the trace of the orthogonalized $\mathbf{U}_{ij}$ tensor.

Table 4. Fractional Atomic Coordinates and Equivalent Atomic Displacement Parameter (U_{eq}) Values in 10^{-3} Å^2 for $Rb_{0.36}Sn_{2.36}Bi_{11.64}Se_{20}$ with Estimated Standard Deviations in Parentheses

	x	y	z	occupancy	U_{eq}[a]
Bi1	0.61199(5)	0.25	0.08172(5)	1	21.0(2)
Bi2	0.85144(5)	−0.25	0.26356(5)	1	20.0(2)
Bi3	0.09208(5)	−0.75	0.45219(5)	1	17.2(2)
Bi4	0.32303(5)	−0.25	0.63387(5)	1	21.8(2)
Bi5/Sn5′	0.82202(7)	−0.25	0.76185(7)	0.775(3)/0.225	27.6(3)
Bi6/Sn6′	0.89463(7)	−0.75	0.00224(6)	0.686(3)/0.314	21.7(3)
Sn1/Bi1′	0.6000(1)	−0.75	0.7854(1)	0.644(3)/0.356	43.2(4)
Rb1	0.498(1)	0.25	0.502(1)	0.182(5)	113(12)
Se1	0.4180(2)	0.25	0.0453(1)	1	19.1(4)
Se2	0.8197(2)	0.25	0.1399(1)	1	19.2(4)
Se3	0.0593(1)	−0.25	0.3272(1)	1	17.2(4)
Se4	0.2878(1)	−0.75	0.5060(1)	1	18.8(4)
Se5	0.5080(2)	−0.25	0.6672(2)	1	46.6(8)
Se6	0.6481(2)	−0.25	0.2233(1)	1	20.4(5)
Se7	0.8851(1)	−0.75	0.4068(1)	1	15.2(4)
Se8	0.6938(2)	−0.75	0.6825(2)	1	23.4(5)
Se9	0.0245(1)	−0.25	0.1112(1)	1	20.1(4)
Se10	0.7644(2)	−0.25	0.8907(1)	1	21.1(4)

[a] U_{eq} is defined as one-third of the trace of the orthogonalized $\mathbf{U}_{ij}$ tensor.

Table 5. Fractional Atomic Coordinates ($y = 0.25$) and Equivalent Atomic Displacement Parameter (U_{eq}) Values in 10^{-3} Å^2 for $Cs_{0.46}Sn_{2.46}Bi_{11.54}Se_{20}$ with Estimated Standard Deviations in Parentheses

	x	*z*	occupancy	U_{eq}[a]
Bi1	0.61230(6)	0.08062(6)	1	16.7(2)
Bi2	0.14887(6)	0.73650(5	1	13.7(2)
Bi3	0.09146(6)	0.45149(5)	1	12.0(2)
Bi4	0.67817(6)	0.36466(6)	1	18.1(2)
Bi5/Sn5′	0.18104(9)	0.23897(9)	0.737(2)/0.263	28.6(3)
Bi6/Sn6′	0.89449(8)	0.00216(7)	0.830(2)/0.170	21.7(2)
Sn1	0.6037(2)	0.7980(2)	0.798(2)	21.8(6)
Bi1′	0.5850(5)	0.7614(4)	0.202	21.8
Cs1	0.4975(6)	0.4985(6)	0.230(7)	91(6)
Se1	0.4189(2)	0.0458(2)	1	16.0(5)
Se2	0.8192(2)	0.1392(1)	1	13.7(5)
Se3	0.9398(2)	0.6723(1)	1	13.4(5)
Se4	0.2865(2)	0.5077(2)	1	16.0(5)
Se5	0.4934(2)	0.3277(4)	1	67.7(2)
Se6	0.3495(2)	0.7768(2)	1	17.0(5)
Se7	0.8853(2)	0.4064(1)	1	10.6(4)
Se8	0.6915(2)	0.6856(2)	1	30.3(7)
Se9	0.9740(2)	0.8884(2)	1	18.6(5)
Se10	0.2345(2)	0.1081(2)	1	24.4(6)

[a] U_{eq} is defined as one-third of the trace of the orthogonalized $\mathbf{U}_{ij}$ tensor.

charge-balanced formula $K_{1-x}Sn_{3-x}Bi_{11+x}Se_{20}$ assuming the formal charges of K^+, Sn^{2+}, Bi^{3+}, and Se^{2-}. After anisotropic refinement the R1 and wR2 values dropped to 3.2% and 5.4%, respectively. The results of the structure refinement and other crystallographic data are given in Tables 1 and 3.

$Rb_{0.36}Sn_{2.36}Bi_{11.64}Se_{20}$. The structure was refined with the model of $K_{1-x}Sn_{3-x}Bi_{11+x}Se_{20}$ as a starting point. Even though Sn was introduced in all the bismuth sites, only sites Bi5 through Bi7 contained statistically significant amounts of Sn. All atoms were refined anisotropically to the final *R* values, R1 = 5.4%, wR2 = 14.7%. The results of the structure refinements are given in Table 1. The fractional atomic coordinates and equivalent isotropic displacement parameters are listed in Table 4.

$Cs_{0.46}Sn_{2.46}Bi_{11.54}Se_{20}$. The structure was refined with the model of $K_{1-x}Sn_{3-x}Bi_{11+x}Se_{20}$ as a starting point. Only sites Bi5 through Bi7 and Sn1 contained statistically significant amounts of Sn and Bi, respectively. High remaining electron density (8.10 e/Å^3) close to the Sn1 site led to a splitting of the mixed occupied site into two distinct positions. Anisotropic refinement dropped the final *R* values to R1 = 5.3%, wR2 = 11.2%. The results of the structure refinements are given in Table 1. The fractional atomic coordinates and equivalent isotropic displacement parameters are listed in Table 5. Selected interatomic distances for all compounds can be found within the Supporting Information.

Results and Discussion

Structure Description. The quaternary phases $A_{1-x}M'_{3-x}Bi_{11+x}Se_{20}$ (A = K, Rb, Cs; M′ = Sn, Pb) crystallize in a new structure type while $A_{1+x}M'_{3-2x}Bi_{7+x}Se_{14}$ adopts the $K_{2.5}Bi_{8.5}Se_{14}$ structure type.[14] These compounds belong to the homologous series $A_m[M_6Se_8]_m[M_{5+n}Se_{9+n}]$ (M = Bi, Sn or Pb) with $n = 3$ and $m = 1$ and 2, respectively. Figures 1 and 2 show a [010] projection of their structures displaying distinct building units of the NaCl[111]-type and NaCl[100]-type, that are derived from the NaCl lattice as a (111) and a (100) cut, respectively. These units, which are highlighted in Figure 3, are infinitely long in the *b*-direction. They are linked side by side so as to form a three-dimensional anionic framework with partially alkali filled tunnels running along the *b*-axis.

Figure 3 compares both structure types which possess the same $[M_8Se_{12}]$ NaCl[111]-type unit (see boxed area) that are four Bi-octahedra thick and two Bi-octahedra high and therefore

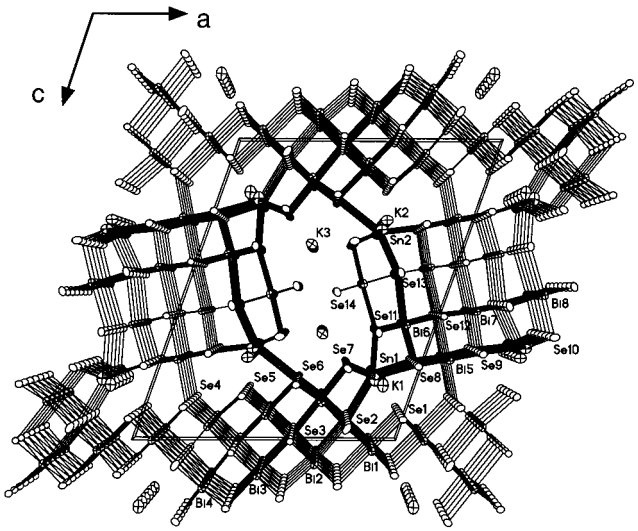

Figure 1. ORTEP representation of the structure of $K_{1.40}Sn_{2.20}Bi_{7.40}Se_{14}$ with atom labeling.

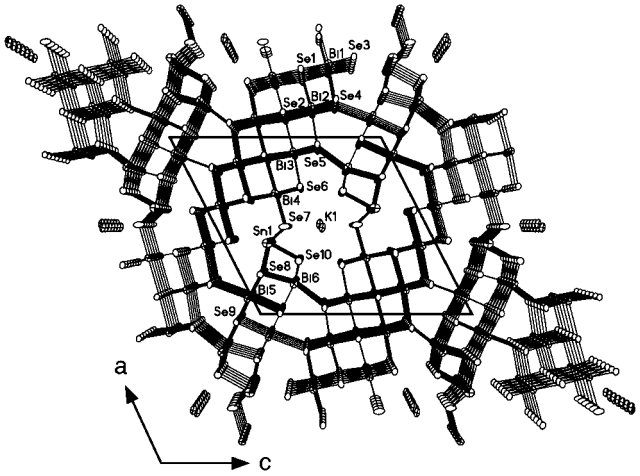

Figure 2. ORTEP representation of the structure of $K_{0.70}Sn_{2.70}Bi_{11.30}Se_{20}$ with atom labeling.

resemble a cut out of a Bi_2Te_3-type layer. Condensation of these units via one octahedron edge results in a step-shaped layer of the formula $[M_{5+n}Se_{9+n}]$ ($n = 3$). The distorted Bi-octahedra have interatomic distances ranging from 2.74 to 3.20 Å for $K_{1.40}Sn_{2.20}Bi_{7.40}Se_{14}$, 2.74−3.11 Å for $K_{0.70}Sn_{2.70}Bi_{11.30}Se_{20}$, 2.76−3.09 Å for $Rb_{0.36}Sn_{2.36}Bi_{11.64}Se_{20}$, and 2.75−3.08 Å for $Cs_{0.46}Sn_{2.46}Bi_{11.54}Se_{20}$. The distances reflect the different extent of Sn/Bi disorder in the step-shaped layers of these compounds. While in $K_{1.40}Sn_{2.20}Bi_{7.40}Se_{14}$ only position Bi2 contains a considerable amount of Sn (11%), mixed occupancies are found for Bi3, Bi4 in $K_{0.70}Sn_{2.70}Bi_{11.30}Se_{20}$, although the fraction of Sn is small, varying from 2.7% to 4.0% Sn. The fraction of Sn in these sites is negligible in $Rb_{0.36}Sn_{2.36}Bi_{11.64}Se_{20}$ and $Cs_{0.46}Sn_{2.46}Bi_{11.54}Se_{20}$.

The two structure types differ in the size of the $[M_6Se_8]$ units that link the stepped $[M_{5+n}Se_{9+n}]$ layers ($n = 3$) via MSe interactions (M = Bi, Sn (Pb)) to a three-dimensional framework. In $A_{1-x}M'_{3-x}Bi_{11+x}Se_{20}$ (A = K, Rb, Cs; M′ = Sn, Pb) these blocks are three M octahedra wide and one octahedron high and therefore very similar to those found in $A_{1-x}M'_{4-x}Bi_{11+x}Se_{21}$[12] and $K_{1-x}Sn_{5-x}Bi_{11+x}Se_{22}$.[13] All metal positions in this block show mixed Bi/M′ occupancy for $A_{1-x}M'_{4-x}Bi_{11+x}Se_{21}$. In contrast, in $K_{1+x}Sn_{3-2x}Bi_{7+x}Se_{14}$ the corresponding $[M_6Se_8]$ units are two M octahedra high in the direction perpendicular to the NaCl[111]-type layers. Here the outer surface of the NaCl[100]-

Table 6. Selected Distances in Å for $K_{1.40}Sn_{2.20}Bi_{7.40}Se_{14}$[a]

Bi1	−Se1	2.805(2)	Bi2	−Se4 × 2	2.8581(9)	Bi3	−Se5 × 2	2.8734(9)
	−Se1 × 2	2.9051(9)		−Se5	2.899(2)		−Se6	2.880(2)
	−Se2 × 2	3.020(1)		−Se3 × 2	3.0388(9)		−Se3	3.015(2)
	−Se4	3.122(2)		−Se2	3.202(2)		−Se3 × 2	3.0525(9)
Bi4	−Se7	2.724(2)	Bi5	−Se12	2.929(1)	Bi6	−Se8	2.732(1)
	−Se6 × 2	2.8734(9)		−Se4	2.935(1)		−Se11 × 2	2.810(1)
	−Se2 × 2	3.090(1)		−Se8 × 2	2.957(1)		−Se12 × 2	3.152(1)
	−Se3	3.175(2)		−Se9 × 2	2.961(1)		−Se13	3.382(2)
Bi7	−Se9	2.731(1)	Bi8	−Se10	2.757(2)	Sn1	−K1	0.66(1)
	−Se13 × 2	2.898(1)		−Se14 × 2	2.767(1)		−Se7 × 2	2.814(1)
	−Se12 × 2	3.018(1)		−Se13 × 2	3.223(1)		−Se11	3.047(2)
	−Se12	3.221(1)		−Se11	3.235(1)		−Se2	3.494(2)
							−Se8 × 2	3.570(2)
							−Se1 × 2	3.717(1)
K1	−Sn1	0.66(1)	Sn2	−K2	0.69(2)	K2	−Sn2	0.69(2)
	−Se1 × 2	3.23(1)		−Se10 × 2	2.836(2)		−Se5 × 2	3.23(1)
	−Se7 × 2	3.28(1)		−Se13	3.002(2)		−Se9 × 2	3.25(1)
	−Se8 × 2	3.31(1)		−Se9 × 2	3.499(2)		−Se10 × 2	3.25(1)
	−Se11	3.44(1)		−Se6	3.588(2)		−Se13	3.47(2)
	−Se2	3.49(2)		−Se5 × 2	3.752(2)		−Se6	3.52(2)
K3	−Se10 × 2	3.420(3)						
	−Se7 × 2	3.441(3)						
	−Se14	3.466(3)						
	−Se14 × 2	3.544(3)						
	−Se11	3.559(4)						
	−Se6	3.573(4)						

[a] Because of the mixed Bi/Sn occupancy on several metal sites, these distances represent only average values.

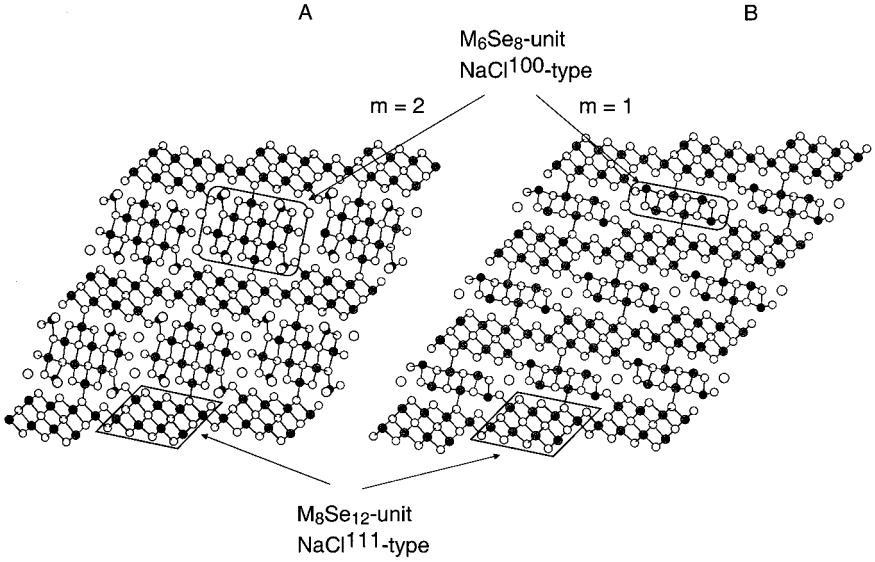

Figure 3. Comparison between two homologues to show close relationship. (A) A larger section of the structure of $K_{1.40}Sn_{2.20}Bi_{7.40}Se_{14}$ viewed down the *b*-axis. (B) The structure of $K_{0.70}Sn_{2.70}Bi_{11.30}Se_{20}$ viewed down the *b*-axis. Small white spheres: Se. Large light-gray spheres: K. Middle-gray spheres: Bi. Dark-gray spheres: Sn. The archetypal $NaCl^{111}$-type and $NaCl^{100}$-type building units are highlighted in both structures.

type block shows considerable mixed K/Sn occupancy with distinct split positions according to the required K−Se and Sn−Se bond distances. We found 23% in the K1 site and 17% in the K2 sites that correspond to the Sn1 and Bi6 site, respectively, in $K_{0.70}Sn_{2.70}Bi_{11.30}Se_{20}$, see Figure 1. A similar disorder of Bi and K is reported for the ternary phase $K_{2.5}Bi_{8.5}Se_{14}$.[14] The metal positions in the interior of the $NaCl^{100}$-type block exhibit extensive disorder of Bi and Sn in the same crystallographic site with 13% Sn in the Bi5 site, 16% Sn in the Bi6 site, and 17% Sn in the Bi7 site. However, the Bi8 site is fully occupied by Bi.

The tricapped prismatic site within the tunnels is fully occupied with K, and its ADP is normal in $K_{1.40}Sn_{2.20}Bi_{7.40}Se_{14}$. In contrast, the corresponding sites in $A_{1-x}Sn_{3-x}Bi_{11+x}Se_{20}$ are only partly occupied, see Table 3, and the observed large ADP of the alkali atoms is caused by positional disorder along the tunnel and possibly "rattling" about their crystallographic site.

Perspective and Classification of the New Quaternary Selenides. $A_{1+x}M'_{3-2x}Bi_{7+x}Se_{14}$ and $A_{1-x}M'_{3-x}Bi_{11+x}Se_{20}$ (A = K, Rb, Cs; M′ = Sn, Pb) are new members of the homologous series $A_m[M_6Se_8]_m[M_{5+n}Se_{9+n}]$ with $n = 3$ and $m = 2$ and $m = 1$, respectively. The close relationship of $K_{1-x}Sn_{3-x}Bi_{11+x}Se_{20}$ to $K_{1-x}Sn_{4-x}Bi_{11+x}Se_{21}$[12] and $K_{1-x}Sn_{5-x}Bi_{11+x}Se_{22}$[13] is obvious from the color scheme depicted in Figure 4. While the $NaCl^{100}$-type block (boxed area) remains the same for all three phases, the latter two (i.e., $n = 4$ and $n = 5$) can be easily derived from $K_{1-x}Sn_{3-x}Bi_{11+x}Se_{20}$ by successively adding SnSe equivalents to the $[M_8Se_{12}]$ layers. One can also imagine compounds with the formulas $K_{1-x}Sn_{2-x}Bi_{11+x}Se_{19}$ ($n = 2$) and $K_{1-x}Sn_{6-x}Bi_{11+x}Se_{23}$ ($n = 6$) that would belong to the series $A_m[M_6Se_8]_m[M_{5+n}Se_{9+n}]$ for $m = 1$. A similar relationship exists between

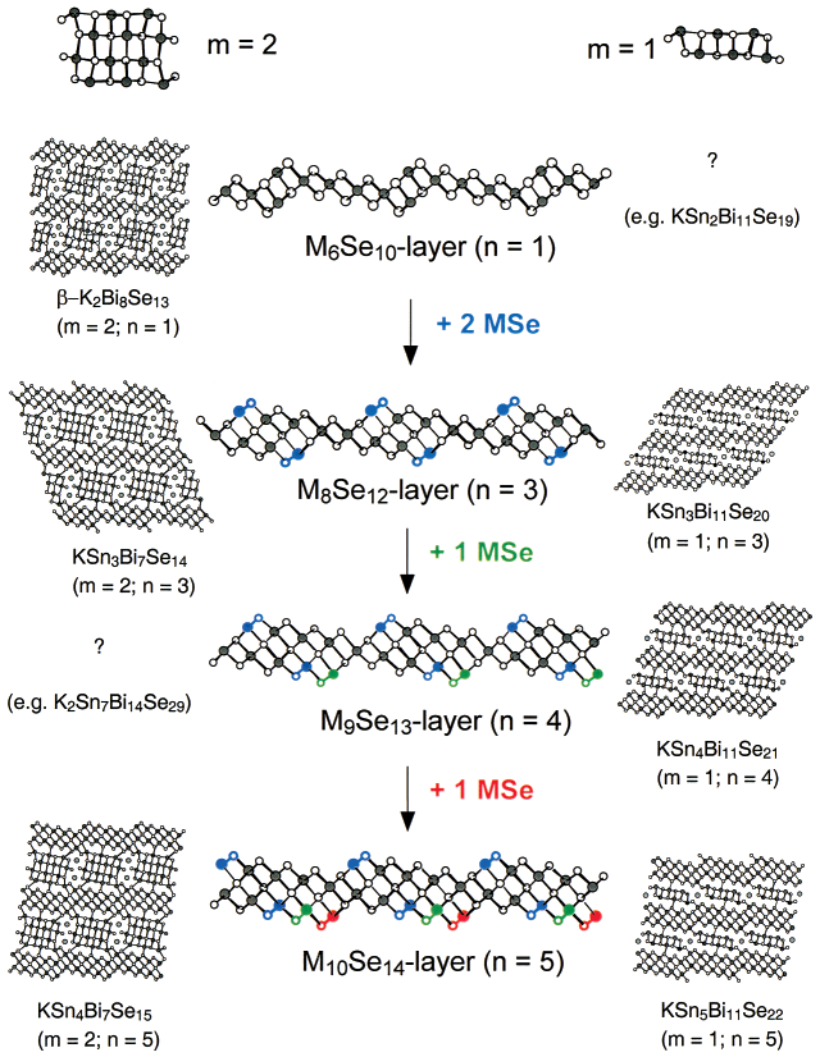

Figure 4. The homologous series $A_m[M_6Se_8]_m[M_{5+n}Se_{9+n}]$. A member generating scheme illustrating successive additions of MSe units to a M_5Se_9 layer. Small white spheres: Se. Large light-gray spheres: K. Middle-gray spheres: M. Question marks are meant to indicate predicted but as of yet undiscovered compositions.

β-$K_2Bi_8Se_{13}$,[6,7] $K_{1+x}Sn_{3-2x}Bi_{7+x}Se_{14}$, and $K_{1+x}Sn_{4-2x}Bi_{7+x}Se_{15}$,[8] which are successive members. They differ by one SnSe unit per formula.

The scheme of Figure 4 places all known members in the same context and offers an easy way to predict new phases by combining known $[M_6Se_8]_m$ blocks and $[M_{5+n}Se_{9+n}]$ layers. Besides varying n to obtain new compounds it would be worth exploring if members with $m > 2$ are also stable. The numerous compounds discovered in the systems K/Sn/Bi/Se and Rb/Sn/Bi/Se[8,12,13,21] suggest strongly that the A/M′/Bi/Se system may be "*infinitely adaptive*".[22] In other words, small variations of the ratio of the starting materials result in new compounds with gradually evolving structural features. The system seems to adjust to a new structure type each time the composition changes rather than form varying mixtures of two or more phases or form solid solutions. The $A_m[M_6Se_8]_m[M_{5+n}Se_{9+n}]$ homology may capture only a fraction of the total number of phases possible, as we have observed compositions which do not belong to the series.[23] It is remarkable that we are able to make pure products of compositions that differ only by one SnSe per formula. We attempted to synthesize the two missing members $Rb_{1+x}M'_{3-2x}Bi_{7+x}Se_{14}$ (M′ = Sn, Pb) but did not succeed; instead we obtained $Rb_{1-x}M'_{3-x}Bi_{11+x}Se_{20}$ with an unknown minority phase.

Charge Transport Properties. Preliminary charge transport measurements of several members of these phases have been carried out. The electrical conductivity of the quaternary selenides described here was measured on polycrystalline ingots and found to be strongly influenced by the ingot preparation conditions. If the molten mixture of the starting materials was quenched, high electrical conductivity, 1700 S/cm, was observed for $K_{1-x}Sn_{3-x}Bi_{11+x}Se_{20}$, and also for $Rb_{1-x}Sn_{3-x}Bi_{11+x}Se_{20}$, 1350 S/cm. For a slowly cooled sample of $K_{1-x}Sn_{3-x}Bi_{11+x}Se_{20}$ (see description in the Experimental Section) we found the much lower electrical conductivity of 520 S/cm at room temperature. For slowly cooled samples, the substitution of K by Cs seems to decrease the electrical conductivity (370 S/cm for $Cs_{1-x}Sn_{3-x}Bi_{11+x}Se_{20}$) while the Pb analogues $K_{1-x}Pb_{3-x}Bi_{11+x}Se_{20}$ (700 S/cm) and $Cs_{1-x}Pb_{3-x}Bi_{11+x}Se_{20}$ (690 S/cm) possess higher electrical conductivity than the Sn compounds. A similar trend is found for $A_{1+x}M'_{3-2x}Bi_{7+x}Se_{14}$, see Table 7. The room

(21) Iordanidis, L.; Mrotzek, A.; Kanatzidis, M. G. Unpublished results.
(22) (a) Anderson, J. S. *J. Chem. Soc., Dalton Trans.* **1973**, *10*, 1107−1115. (b) Swinnea, J. S.; Steinfink, H. *J. Solid State Chem.* **1982**, *41*, 114−123. (c) Mercurio, D.; Parry, B. H.; Frit, B.; Harburn, G.; Williams, R. P.; Tilley, R. J. D. *J. Solid State Chem.* **1991**, *92*, 449−459.
(23) Mrotzek, A.; Kanatzidis, M. G. *Chem. Commun.* **2001**, *17*, 1648−1649.

Table 7. Thermoelectric Properties, Band Gaps, and Melting Points for Members of the $A_m[M_6Se_8]_m[M_{5+n}Se_{9+n}]$ Series

compd	σ (S/cm)	S_{300K} (μV/K)	E_g (eV)	mp (°C)
β-$K_2Bi_8Se_{13}$[6,7]	250	−200	0.59	672
$K_{2.5}Bi_{8.5}Se_{14}$[14]	150	−100	0.56	692
$K_{1+x}Sn_{3-2x}Bi_{7+x}Se_{14}$	2000	−45	*c*	689
$K_{1+x}Pb_{3-2x}Bi_{7+x}Se_{14}$	630	−32	0.56	692
$Cs_{1+x}Sn_{3-2x}Bi_{7+x}Se_{14}$	200	−48	0.40	669
$Cs_{1+x}Pb_{3-2x}Bi_{7+x}Se_{14}$	350	−56	0.62	716
$K_{1+x}Sn_{4-2x}Bi_{7+x}Se_{15}$[8]	110	−70	0.39	662
$K_{1-x}Sn_{3-x}Bi_{11+x}Se_{20}$[a]	1700	−16	*c*	676
$K_{1-x}Sn_{3-x}Bi_{11+x}Se_{20}$[b]	520	−68	0.30	676
$K_{1-x}Pb_{3-x}Bi_{11+x}Se_{20}$[a]	700	−49	0.55	694
$Rb_{1-x}Sn_{3-x}Bi_{11+x}Se_{20}$[a]	1350	−25	*c*	675
$Rb_{1-x}Pb_{3-x}Bi_{11+x}Se_{20}$[a]	1060	−46	0.54	667
$Cs_{1-x}Sn_{3-x}Bi_{11+x}Se_{20}$[b]	370	−69	0.40	668
$Cs_{1-x}Pb_{3-x}Bi_{11+x}Se_{20}$[b]	690	−91	*c*	714
$K_{1-x}Sn_{4-x}Bi_{11+x}Se_{21}$[12]	1800	−52	*c*	673
$K_{1-x}Sn_{5-x}Bi_{11+x}Se_{22}$[13]	450	−43	*c*	680

[a] Quenched. [b] Slowly cooled. [c] Could not be determined reliably due to the high absorption from mid gap states.

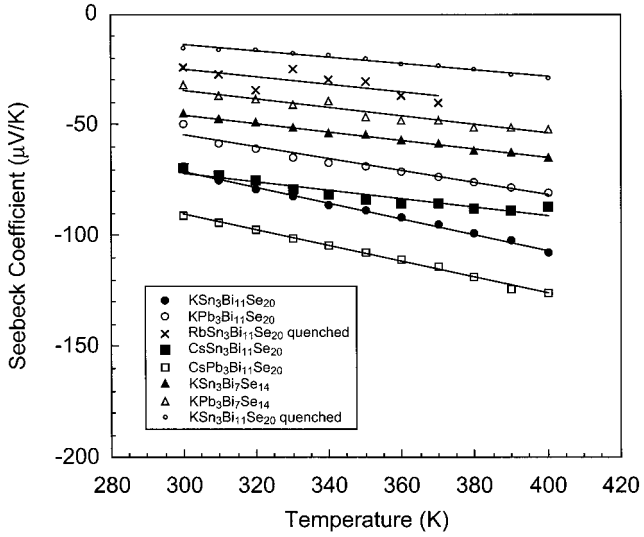

Figure 5. Variable-temperature thermoelectric power data of polycrystalline ingots of $K_{1+x}M'_{3-2x}Bi_{7+x}Se_{14}$ and $A_{1-x}M'_{3-x}Bi_{11+x}Se_{20}$ (A = K, Rb, Cs; M' = Sn, Pb).

temperature values for slowly cooled $K_{1+x}Sn_{3-2x}Bi_{7+x}Se_{14}$ (2000 S/cm), $K_{1+x}Pb_{3-2x}Bi_{7+x}Se_{14}$ (630 S/cm), $Cs_{1+x}Sn_{3-2x}Bi_{7+x}Se_{14}$ (200 S/cm), and $Cs_{1+x}Pb_{3-2x}Bi_{7+x}Se_{14}$ (350 S/cm) are higher than the value reported for the isostructural ternary, $K_{2.5}Bi_{8.5}Se_{14}$. The former values are comparable to those of quenched $K_{1-x}Sn_{3-x}Bi_{11+x}Se_{20}$ and slowly cooled $K_{1-x}Pb_{3-x}Bi_{11+x}Se_{20}$. The high conductivity of quenched samples is attributed to the generation of a large number of defects in the structure, whose exact nature is not known but can be speculated to be M/Se anti-site defects or Se vacancies.

Table 7 summarizes room temperature values for thermopower, electrical conductivity, band gaps, and melting points for $A_{1+x}M'_{3-2x}Bi_{7+x}Se_{14}$, $A_{1-x}M'_{3-x}Bi_{11+x}Se_{20}$ (A = K, Rb, Cs; M' = Sn, Pb), $K_{2.5}Bi_{8.5}Se_{14}$, β-$K_2Bi_8Se_{13}$, $K_{1+x}Sn_{4-2x}Bi_{7+x}Se_{15}$, $K_{1-x}Sn_{4-x}Bi_{11+x}Se_{21}$, and $K_{1-x}Sn_{5-x}Bi_{11+x}Se_{22}$. All materials are n-type semiconductors. The thermopower was measured between 300 and 400 K on oriented polycrystalline aggregates of $A_{1+x}M'_{3-2x}Bi_{7+x}Se_{14}$ and $A_{1-x}M'_{3-x}Bi_{11+x}Se_{20}$. These compounds possess moderate negative Seebeck coefficients with a nearly linear dependence, see Table 7 and Figure 5. The negative values indicate n-type behavior with electrons as the dominant charge carriers. With rising temperature from 300 to 400 K the absolute value of the negative Seebeck coefficient increases from −45 to −62 μV/K for $K_{1+x}Sn_{3-2x}Bi_{7+x}Se_{14}$ and −32 to −52 μV/K for $K_{1+x}Pb_{3-2x}Bi_{7+x}Se_{14}$, respectively. The Cs analogues have slightly higher thermopower at room temperature with −48 μV/K ($Cs_{1+x}Sn_{3-2x}Bi_{7+x}Se_{14}$) and −56 μV/K ($Cs_{1+x}Pb_{3-2x}Bi_{7+x}Se_{14}$). Such moderately low values may be reasonable considering the high electrical conductivity of these sample. In comparison to the ternary selenide $K_{2.5}Bi_{8.5}Se_{14}$, the partial substitution of K and Bi by Sn (Pb) causes a drastic drop in the thermopower from −100 μV/K at room temperature. As found for $K_{2.5}Bi_{8.5}Se_{14}$ its properties are sensitive to the preparation method; therefore we can expect that the quaternary analogue would behave similarly.

Slowly cooled samples of $K_{1-x}Sn_{3-x}Bi_{11+x}Se_{20}$ exhibit a linearly rising absolute Seebeck value from −68 μV/K at 300 K to −107 μV/K at 400 K. However, we observed much lower thermopower for the quenched sample. The low values starting from −16 to −28 μV/K correspond to the higher electrical conductivity observed for this sample, see Table 7. Quenched $Rb_{1-x}Sn_{3-x}Bi_{11+x}Se_{20}$ behaves similarly, exhibiting a low thermopower of −26 μV/K at 300 K that rises to −35 μV/K at 400 K. By comparison, the slowly cooled sample of $Cs_{1-x}Sn_{3-x}Bi_{11+x}Se_{20}$ possesses higher thermopower (−69 μV/K increasing to −92 μV/K) consistent with its lower electrical conductivity of 370 S/cm. Substitution of Sn by Pb led analogously to $K_{1+x}Pb_{3-2x}Bi_{7+x}Se_{14}$ to an about 30% reduced thermopower for

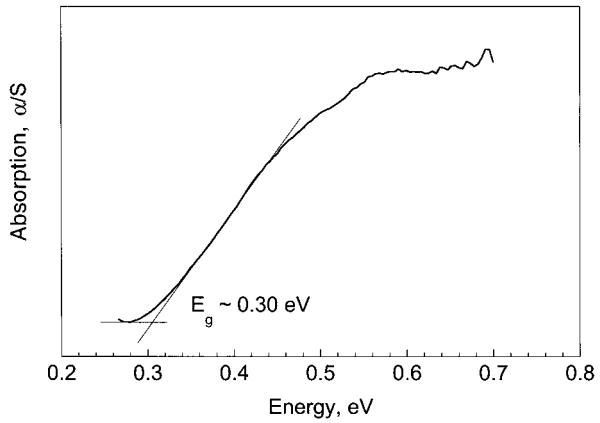

Figure 6. Infrared absorption spectrum of $K_{1-x}Sn_{3-x}Bi_{11+x}Se_{20}$ obtained at room temperature. The energy band gap is indicated in the spectrum.

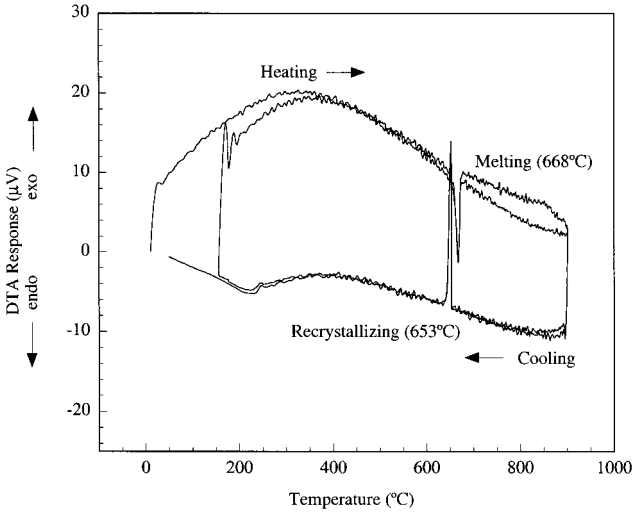

Figure 7. Differential thermogram of $Cs_{1-x}Sn_{3-x}Bi_{11+x}Se_{20}$ showing melting and recrystallization events. Heating/cooling rate of 10 °C/min.

$K_{1-x}Pb_{3-x}Bi_{11+x}Se_{20}$ (-49 μV/K at 300 K). The thermopower of $Rb_{1-x}Sn_{3-x}Bi_{11+x}Se_{20}$ (-46 μV/K at 300 K) is comparable to the latter, see Table 7. In contrast, the Pb analogue $Cs_{1-x}Pb_{3-x}Bi_{11+x}Se_{20}$ shows values rising from -91 μV/K at 300 K to -126 μV/K at 400 K, the highest thermopower observed for any $A_{1-x}M'_{3-x}Bi_{11+x}Se_{20}$ (A = K, Rb, Cs; M′ = Sn, Pb).

Energy Gaps and Thermal Properties. The infrared absorption spectra of $A_{1+x}M'_{3-2x}Bi_{7+x}Se_{14}$ and $A_{1-x}M'_{3-x}Bi_{11+x}Se_{20}$ (A = K, Rb, Cs; M′ = Sn, Pb) were recorded at room temperature in the range 0.1−0.7 eV. The optical band gaps of $K_{1+x}Sn_{3-2x}Bi_{7+x}Se_{14}$, $Rb_{1-x}Sn_{3-x}Bi_{11+x}Se_{20}$, and $Cs_{1-x}Pb_{3-x}Bi_{11+x}Se_{20}$ could not be determined reliably. However, for $K_{1+x}Pb_{3-2x}Bi_{7+x}Se_{14}$, $Cs_{1+x}M'_{3-2x}Bi_{7+x}Se_{14}$, $K_{1-x}M'_{3-x}Bi_{11+x}Se_{20}$, $Rb_{1-x}Pb_{3-x}Bi_{11+x}Se_{20}$, and $Cs_{1-x}Sn_{3-x}Bi_{11+x}Se_{20}$ we were able to observe optical band gaps between ~0.3 eV (see Figure 6) and 0.6 eV. The narrow band gaps of these quaternary selenides are consistent with the observed charge transport behavior described above.

According to DTA experiments $A_{1+x}Sn_{3-2x}Bi_{7+x}Se_{14}$ and $A_{1-x}Sn_{3-x}Bi_{11+x}Se_{20}$ (A = K, Rb, Cs) melt and recrystallize without structural change (the melting points are listed in Table 7), while the analogous lead compounds melt incongruently. A typical differential thermogram is shown in Figure 7 for $Cs_{1-x}Sn_{3-x}Bi_{11+x}Se_{20}$. The well-defined melting and crystallization events and their close proximity reflect the essentially congruent melting behavior of the material.

Concluding Remarks

The exploration of the system A/M′/Bi/Se (A = K, Rb, Cs; M′ = Sn, Pb) reported here and elsewhere[8,12,13] leads to the suggestion that it may be "infinitely adaptive". The existence of the grand homologous series $A_m[M_6Se_8]_m[M_{5+n}Se_{9+n}]$ that defines a certain fraction of the possible compounds seems clear at this stage. The phases $A_{1+x}M'_{3-2x}Bi_{7+x}Se_{14}$ and $A_{1-x}M'_{3-x}Bi_{11+x}Se_{20}$ (A = K, Rb, Cs; M′ = Sn, Pb) were predicted and synthesized as new members of this series. All members of the homologous series are constructed from the basic $NaCl^{111}$- and the $NaCl^{100}$-type modules whose sizes vary according to *n* and *m*. The phases $A_{1+x}M'_{3-2x}Bi_{7+x}Se_{14}$ and $A_{1-x}M'_{3-x}Bi_{11+x}Se_{20}$ are n-type narrow band gap semiconductors with moderate electrical conductivity and thermopower. The pursuit of new members of the series continues.

Acknowledgment. Financial support from the Office of Naval Research (Grant No. N00014-98-1-0443) and the Deutsche Forschungsgemeinschaft is gratefully acknowledged. This work made use of the SEM facilities of the Center for Advanced Microscopy at Michigan State University.

Supporting Information Available: X-ray crystallographic data for $K_{1.40}Sn_{2.20}Bi_{7.40}Se_{14}$, $K_{0.70}Sn_{2.70}Bi_{11.30}Se_{20}$, $Rb_{0.36}Sn_{2.36}Bi_{11.64}Se_{20}$, and $Cs_{0.46}Sn_{2.46}Bi_{11.54}Se_{20}$, in CIF format. This material is available free of charge via the Internet at http://pubs.acs.org.

IC010285W